Dyes and Pigments 246 (2026) 113329

Contents lists available at ScienceDirect

Dyes and Pigments

journal homepage: www.elsevier.com/locate/dyepig

Organic luminescent radicals with blue-green emission for organic light-emitting diodes

Marco Zechner [a], Suman Mallick [a,*], Max Schmallegger [b], Daniele Padula [c], Thomas Rath [a], Gregor Trimmel [a,**]

[a] Institute for Chemistry and Technology of Materials, NAWI Graz, Graz University of Technology, Stremayrgasse 9, 8010, Graz, Austria
[b] Institute of Physical and Theoretical Chemistry, NAWI Graz, Graz University of Technology, Stremayrgasse 9, 8010, Graz, Austria
[c] Dipartimento di Biotecnologie, Chimica e Farmacia, Università di Siena, via A. Moro 2, 53100, Siena, Italy

ARTICLE INFO

Keywords:
Organic radicals
OLEDs
Fluorescence
Aggregation induced emission

ABSTRACT

Stable organic light emitting radicals are promising candidates for high-efficiency organic light emitting diodes (OLEDs). For radicals, both the ground state and the excited state are doublet states, thus, circumventing the non-radiative energy loss of the spin forbidden triplet state. The aim of this work was to synthesize new, stable, light-emitting organic radicals with emission in the visible range, which is ideally shifted towards the blue region of the spectrum in the solid state by utilizing aggregation induced emission (AIE) properties. The synthesis of these light-emitting radicals was achieved via two different synthetic pathways. In the first series of molecules, based upon an anthracene core structure, three precursors and two final radicals were obtained. For the second series, based upon a trityl core structure, also three precursors and two final products were synthesized, with tetraphenylethylene (TPE), mesitylene and pyrene being used as substituents. All of the final products displayed photoluminescent and paramagnetic properties. The radicals exhibit fluorescence emission in the range from 383 nm to 529 nm, with solid-state quantum yields of up to 16.5 %, showcasing the high potential of this approach to create new fluorophores for high-performance multicolored OLEDs in the near future.

1. Introduction

OLEDs already have established themselves in various technological applications, such as displays for mobile devices and television [1]. Despite significant improvements in terms of power efficiency, color purity and cost effectiveness over other display technologies, OLEDs still allow the potential for further enhancements. Due to the closed-shell structure of the fluorescent molecules, only 25 % of the excitons are in a singlet state and the remaining 75 % of the excitons are in a triplet state [2]. For the triplet excitons, it is spin forbidden to return to the ground state and they usually exhibit a non-radiative energy loss [3]. In turn, this limits the internal quantum efficiency (IQE) to 25 % [4], thus yielding a maximum external quantum efficiency (EQE) of just 5–7.5 % [5].

To circumvent these issues, several solutions have been proposed. For one, phosphorescent OLEDs can achieve a theoretical IQE value of up to 100 % since they also allow the usage of the triplet energy. Singlet excitons can be converted into triplet excitons via inter-system crossing (ISC). However, new problems arise, as these devices rely on the use of heavy metals such as Ir and Pt [6,7]. These materials are not only expensive but also harmful to the environment and thus cannot be seen as promising candidates for future development.

An encouraging attempt to improve the properties of these organic emitters has already been carried out with the exploitation of thermally activated delayed fluorescence (TADF) type emitters [8]. The proper design of an organic molecule can allow for the energy gap between the first singlet and triplet excited states to be small enough (<0.1 eV) to enable thermal upconversion from the triplet to the singlet state via reverse intersystem crossing (RISC) [4,9]. These types of molecules have already been successfully explored for conventional non-radical OLEDs yielding near-optimum IQE values [10].

An important milestone towards an improved efficiency of OLEDs was set in 2015 by Li et al. [11] In their work, they used an organic open-shell molecule as the emitter enabling them to obtain a theoretical IQE of 100 % [12]. In the case of open-shell molecules (Fig. 1), the energetically highest occupied orbital is only occupied by one electron,

* Corresponding author.
** Corresponding author.
E-mail addresses: mallick@tugraz.at (S. Mallick), gregor.trimmel@tugraz.at (G. Trimmel).

https://doi.org/10.1016/j.dyepig.2025.113329
Received 29 August 2025; Received in revised form 30 September 2025; Accepted 11 October 2025
Available online 13 October 2025

also referred to as singly occupied molecular orbital (SOMO). Its energy lies between the HOMO and LUMO [13], with the monoradical having a total spin quantum number of S = ½. If an excitation of this electron occurs to the LUMO, there is no electron in the SOMO left, leaving this orbital unoccupied [14]. Since there is no change in the spin quantum number, the transition back from the LUMO to the SOMO is 100 % spin allowed [15]. Due to the fact, that one single electron possesses two possible spin states, it is called a doublet [16]. Thus, the photoluminescence stems from the relaxation of the excited D_1 state to the D_0 ground state. The D_0 to D_1 excitation can be viewed as a mainly HOMO-SOMO and in certain cases also as SOMO-LUMO transition, with the energy differences of the transitions being non-degenerate [17].

Upon taking a closer look as to why these transitions are non-degenerate, it is evident that due to the unpaired electron, the spin degeneracy of the orbitals is lifted via various spin exchange interactions [18]. Following these interactions, the orbitals split into two sub-orbitals with varying energy levels [16]. Hence there are two SOMO sub-orbitals, one of them being occupied by one unpaired electron (SOMO α), whereas the second one is unoccupied (SOMO β) and thus referred to as a singly unoccupied molecular orbital (SUMO).

In an attempt to further improve the stability of these organic radicals, a non-Aufbau electronic configuration was suggested (Fig. 2) [19,20]. In this case, the HOMO of the donor group serves as the highest occupied orbital rather than the SOMO of the radical, whose energetic level now lies below the doubly occupied orbital, preventing reactions with the SOMO [21,22].

However, these types of radicals still had a lower photoluminescence quantum efficiency (PLQE) when compared to the conventional closed-shell materials. The lower values have been attributed mainly to the alternant and symmetric structure of the monoradicals. If both of these properties are present, the HOMO-SOMO and SOMO-LUMO transitions are degenerative. The light emission is overshadowed by internal non-radiative conversion processes from D_1 to D_0. It should be noted that the breakage of the alternant symmetry of these monoradicals leads to an increased extinction coefficient for the D_0 to D_1 transition and a higher transition dipole moment of the D_1 state and thus also leads to a higher PLQE value [23].

The usage of non-alternant donor-acceptor (D-A) radical systems enables straightforward functionalization of otherwise non-emissive alternant radical structures via simple substitution reactions. Carbazole and its derivatives are one of the most studied structures [24,25]. Ideally an electron-rich, asymmetric molecule with a high HOMO is attached to the monoradical, thus reducing the degeneracy of the frontier orbitals in order to obtain the highest luminescence values [26]. If a D-A radical type, however, is derived from an alternant hydrocarbon functional group as a substitute, there still remains an overall alternancy in the structure. These alternant D-A type radicals suffer from the degeneration of the functional group-HOMO to radical-SOMO and radical-SOMO to functional group-LUMO transitions. An example of such a molecule is the stable mesityl-substituted tri(9-anthryl)methyl (TAntM) radical, which is non-luminescent [27,28].

Blue/green emitting radicals are not yet reported, which are crucial for white light displays. Herein, we attempt to synthesize new derivatives to fulfill this requirement, based upon the tris (2,4,6-trichlorophenyl)methane (TTM) and the TAntM core structures. By attempting to replace chlorine with bromine atoms on one of the phenyls, we attempt to get a higher control over the attachment of electron-donating moieties. Furthermore, another pathway based upon the TAntM core, which displays not only high stability, but also provides the opportunity to avoid halogens is explored. Suzuki-, Sonogashira and Buchwald-Hartwig reactions should allow for a straightforward attachment of substitutes, such as TPE, pyrene and mesitylene. These reagents should further increase the stability of the radicals due to a larger steric hindrance and an increased π-delocalization over their aromatic moieties. Counteracting the expected decrease in LUMO energy, TPE and pyrene are chosen, in order to shift the emission wavelength towards the blue region of the UV–Vis spectrum, which is necessary for developing white light emission. Additionally, these substitutes might also allow for AIE, which could provide interesting new possibilities for open-shell molecules in OLED devices.

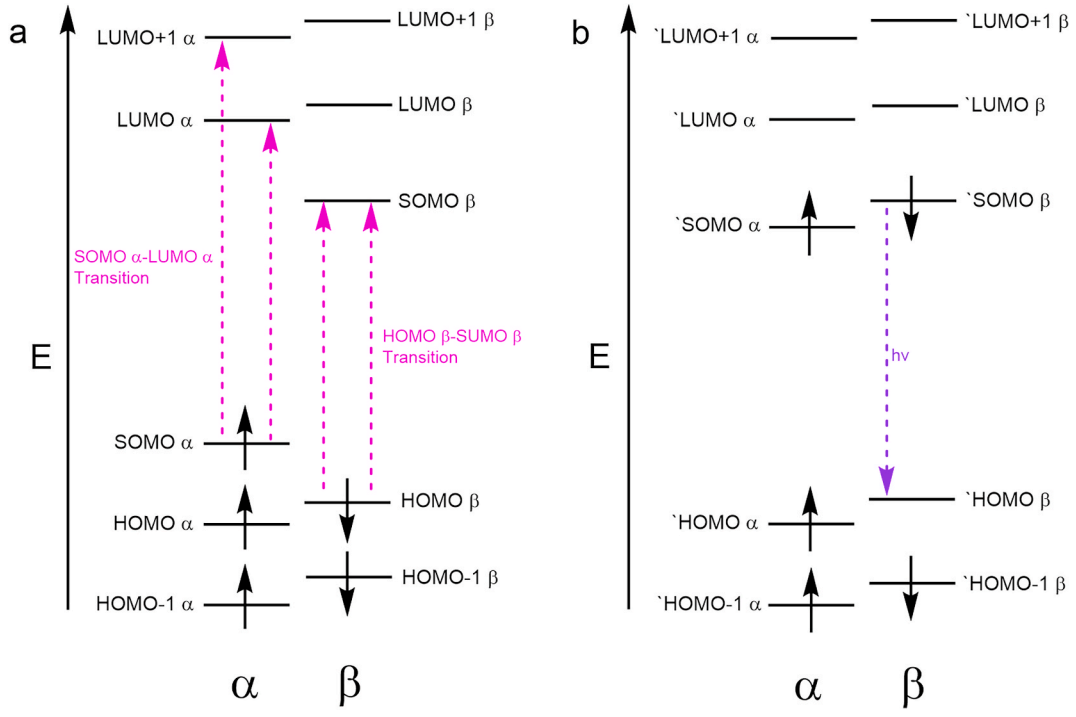

Fig. 1. Emission process and exciton formation mechanism of monoradicals. (a) The frontier molecular orbital diagram of monoradicals in the ground state (D_0) and (b) in the first excited state (D_1). Due to the fact that the electronic configuration is different from the D_0 state, the orbitals (e.g. HOMO), are marked (e.g. 'HOMO) in the D_1 state.

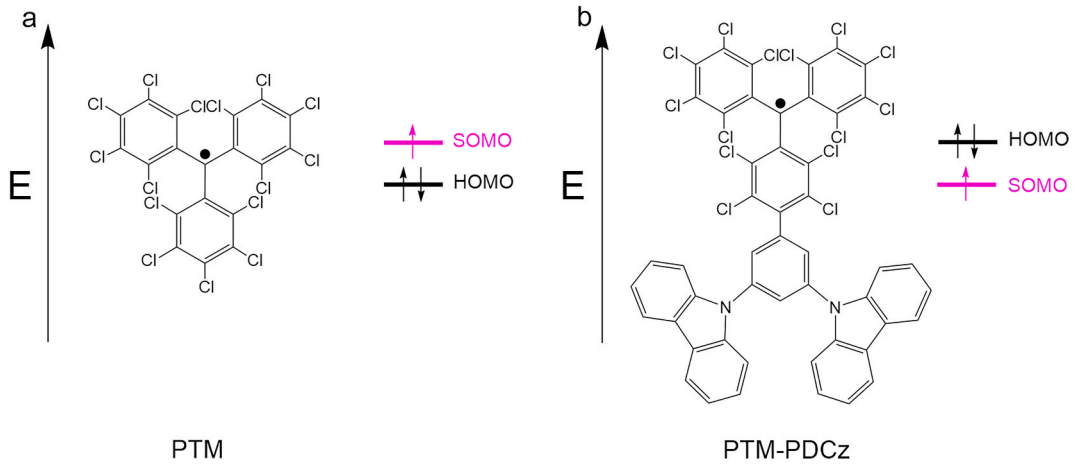

Fig. 2. MO scheme for two monoradicals, with (a) Aufbau-structure of PTM and (b) Non-Aufbau structure of PTM-PDCz.

2. Experimental section

2.1. Materials and methods

TLCs were performed with silica gel 60 on aluminum sheets from Merck. Signals were detected visually under a UV lamp at a wavelength of 254 nm.

^{1}H and ^{13}C NMR spectra were recorded on a Bruker Avance III 300 MHz. Deuterated solvents, such as $CDCl_3$, CD_2Cl_2 were purchased from EurisoTop GmbH. The spectra were referenced against the TMS peak of the deuterated solvent if not otherwise stated. The obtained data are evaluated with the MestReNova program from Mestrelab Research.

APCI measurements were carried out on an Advion Expression CMS with nitrogen as carrier gas and the data was processed using the software Advion Mass Express.

MALDI-TOF measurements were done on a "MALDI micro–MX Mass Spectrometer" from Waters Micromass. As matrices, dithranol or *trans*-2-[3-[4-(*tert*-butyl)phenyl]-2-methyl-2-propenylidene] malononitrile (DCTB) were used (10 mg/ml in THF). Sample concentration 1–2 mg/ml in DCM with a ratio of matrix: sample of 7 μl: 2 μl (7/2; v/v). All spectra were externally calibrated with a polyethylene glycol standard (5 mg/ml in THF). The spectra were interpreted using the MassLynx Software V4.1 from Micromass/Waters.

EI-DI measurements were done on a "JMS-T2000GC AccuTOF GC-Alpha" Time of flight Mass Spectrometer from JEOL. The sample was inserted as a solid in a glass capillary via a direct inlet probe system (DIP) into the MS (temperature: 30 °C–450 °C; ionizing voltage: 70 eV; ion source temperature: 250 °C; calibration: PFTBA (Heptacosa); software: msAxel data processing).

Flash column chromatography was done using a Biotage® selekt column chromatography instrument. Chromabond flash 14–40 μm SiOH columns of appropriate sizes were used (20–120 g). The product mixture was dissolved and an appropriate amount of silica gel was added, the solvent was removed under reduced pressure. The resulting slurry was transferred in a pre-column already packed with silica gel.

Continuous-wave EPR (CW-EPR) spectra were recorded on a Bruker X-band spectrometer (EMX, 100 kHz field modulation) at ambient temperature with 0.2 mT field modulation amplitude.

UV–Vis spectra measurements were performed on a Shimadzu UV-1800 spectrometer. The measurements are carried out within the wavelength range of 220–1100 nm. The samples are diluted in THF as the standard solvent and measured in 1 cm quartz glass cuvettes.

Fluorescence emission and excitation spectra were recorded on a Fluorolog 3® spectrofluorometer from Horiba Scientific equipped with a R2658 photomultiplier from Hamamatsu.

Quantum yields of the solid-state and solution samples were measured on a Fluorolog 3® spectrofluorometer from Horiba Scientific using a Quanta-φ integrating sphere from Horiba.

All chemicals were either used from already existing stockpiles in our laboratories or purchased from common commercial chemical suppliers, usually Sigma Aldrich, BLDpharm and TCI, among others. These chemicals were, unless otherwise stated, used without any further purification. The anhydrous DCM was prepared by distillation over P_4O_{10} and the anhydrous THF was prepared by distillation over lithium aluminium hydride ($LiAlH_4$).

2.2. 10-(dibromomethylene)anthracen-9(10H)-one (2)

Anthraquinone (5.27 g, 25.3 mmol) and tetrabromomethane (10.86 g, 32.8 mmol) were both added to a dry reaction vessel. After the addition, the flask was evacuated and filled with nitrogen a total of three times. A syringe was used to add DCM (300 mL) to the flask. The mixture was stirred for 10 min in an ice bath at 0 °C. Followed by the dropwise addition of $P(O–Et)_3$ (10.5 mL, 60.7 mmol). Then the reaction mixture was warmed to room temperature and stirred overnight for 18 h. The reaction was quenched by the addition of water. The organic layer was washed with brine, a total of three times. Upon removal of the solvent in vacuum, the raw product was purified via column chromatography (cyclohexane:ethyl acetate = 9:1 to 5:1). Finally, compound **2** was obtained as a white-pinkish solid (4685 mg, 12.87 mmol, 51 %) ^{1}H NMR (300 MHz, $CDCl_3$) δ 8.09 (t, J = 6.0 Hz, 4H), 7.53 (tdd, J = 15.1, 10.7, 4.3 Hz, 4H).^{13}C NMR (76 MHz, $CDCl_3$) δ 185.19, 138.20, 136.66, 132.49, 130.97, 128.76, 128.52, 126.68, 93.57. MS (APCI) calcd. $C_{15}H_8Br_2O^+$ [M + H$^+$] m/z: 362.90 found: 362.8.

2.3. 10-(bis(4-(1,2,2-triphenylvinyl)phenyl)methylene)anthracen-9(10H)-one (3)

Compound **2** (285 mg, 0.783 mmol), [4-(triphenylvinyl)phenyl] boronic acid pinacol ester (1050 mg, 2.29 mmol) and K_2CO_3 (560 mg, 3.99 mmol) were added to a reaction vessel. The flask was evacuated and filled with nitrogen twice. After this, $Pd(PPh_3)_4$ (88.0 mg, 0.0762 mmol) was added. Afterwards, the flask was again evacuated and subsequently flooded with nitrogen twice. Finally, the solvent (6 mL THF: H_2O = 10:1) was put into the flask with a syringe. The solution was heated in an oil bath at 70 °C over the weekend for three days. After letting the reaction mixture cool down to room temperature, the solvent was removed under vacuum and the solids were redissolved in ethyl acetate. The organic layer was washed with brine a total of two times and the solvent was again removed under vacuum. The raw product was purified via column chromatography (cyclohexane:ethyl acetate = 10:1 to 9:1) to obtain compound **3** as an orange-brown solid (533 mg, 0.615

mmol, 79 %). ^{1}H NMR (300 MHz, CD_2Cl_2) δ 8.07 (d, J = 7.4 Hz, 2H), 7.34 (t, J = 7.2 Hz, 2H), 7.26–6.97 (m, 34H), 6.93 (s, 8H); ^{13}C NMR (76 MHz, $CDCl_3$) δ 185.90, 146.22, 143.64, 143.60, 143.45, 142.64, 141.32, 140.91, 140.38, 139.52, 132.88, 131.40, 131.34, 131.31, 131.26, 130.44, 130.32, 129.30, 128.80, 127.67, 127.18, 126.62, 126.53, 126.49, 126.41, 26.92. MS (MALDI) calcd. $C_{67}H_{46}O^+$ [M^+] *m/z*: 866.3549; found: 866.3535.

2.4. 10-(di(pyren-1-yl)methylene)anthracen-9(10H)-one (4)

Compound **2** (1016 mg, 2.83 mmol) and pyren-1-ylboronic acid (2023 mg, 8.22 mmol) were added to a flask with a magnetic stirring bar. The flask was evacuated and filled with nitrogen twice. After this, $Pd(PPh_3)_4$ (318 mg, 0.275 mmol) was added to the flask, which was again evacuated and flooded with nitrogen twice afterwards. This was followed by the addition of 30 mL of toluene: 2 M Na_2CO_3 = 5:1. The solution was heated in an oil bath at 90 °C for 48 h. After letting the reaction mixture cool down to room temperature, the solvent was removed under vacuum and redissolved in DCM. The organic layer was washed with brine and the remaining solvent was used to prepare a slurry for column chromatography (cyclohexane:ethyl acetate = 15:1) the desired product was obtained as a brown solid (397 mg, 0.65 mmol, 23 %). ^{1}H NMR (300 MHz, $CDCl_3$) δ 8.68 (d, J = 9.2 Hz, 2H), 8.20 (dd, J = 14.1, 7.2 Hz, 8H), 8.08–7.88 (m, 10H), 7.21 (d, J = 7.9 Hz, 2H), 7.11 (t, J = 7.2 Hz, 2H), 6.70 (t, J = 7.4 Hz, 2H); ^{13}C NMR (76 MHz, $CDCl_3$) δ 131.18, 128.91, 128.22, 127.76, 126.78, 126.35, 125.69, 125.48, 125.37, 125.12. MS (MALDI) calcd. $C_{47}H_{26}O^+$ [M^+] *m/z*: 606.1984; found: 606.1925.

2.5. 10-(bis(4-(1,2,2-triphenylvinyl)phenyl)methylene)-9-(4-(1,2,2-triphenylvinyl)phenyl)-9,10-dihydroanthracen-9-ol (5)

1-(4-Bromophenyl)-1,2,2-triphenylethene (233 mg, 0.57 mmol) was added to a dry reaction vessel with a magnetic stirring bar. After evacuating the flask three times, 2 mL of dry THF was added and the mixture was cooled down to −78 °C. 2.5 M n-BuLi (0.2 mL) was added dropwise, and the reaction mixture immediately turned to a yellow color. The mixture was stirred at this temperature for 30 min. Compound **3** (120 mg, 0.14 mmol) in 5 mL of dry THF, was added dropwise and the reaction was slowly let to warm up to room temperature. After further stirring for 3 h, the reaction was quenched with ice and dissolved in DCM. The mixture has been washed with brine and subjected to column chromatography (cyclohexane: ethyl acetate = 15:1 to 5:1) to obtain the desired product as a light yellow solid (117 mg, 0.098 mmol, 70 %). ^{1}H NMR (300 MHz, $CDCl_3$) δ 7.91 (d, J = 7.5 Hz, 2H), 7.28 (s, 1H), 7.23 (s, 1H), 7.17–6.95 (m, 36H), 6.91–6.70 (m, 18H), 6.49 (d, J = 7.7 Hz, 4H), 6.36 (dd, J = 16.3, 8.9 Hz, 3H). ^{13}C NMR (76 MHz, $CDCl_3$) δ 143.84, 143.76, 143.37, 143.22, 143.09, 142.01, 141.09, 140.88, 140.74, 139.99, 139.93, 139.41, 136.36, 133.57, 131.44, 131.36, 131.25, 131.16, 130.93, 130.84, 128.87, 128.78, 127.82, 127.66, 127.57, 127.51, 127.43, 127.02, 126.54, 126.46, 126.33, 125.73, 123.27. MS (MALDI) calcd. $C_{93}H_{66}O^+$ [M^+] *m/z*: 1198.5114; found: 1198.5188.

2.6. 10-(bis(4-(1,2,2-triphenylvinyl)phenyl)methylene)-9-mesityl-9,10-dihydroanthracen-9-ol (6)

A dry reaction vessel with a magnetic stirring bar was evacuated a total of three times. Mesityl bromide (0.1 mL) and 2.5 mL of dry THF were added, and the mixture was cooled down to −78 °C. 2.5 M n-BuLi (0.2 mL) was added dropwise. The mixture was stirred at the same temperature for 30 min. Compound **3** (90 mg, 0.10 mmol), in 5 mL of dry THF was added dropwise and the reaction was slowly let to warm up to room temperature. After further stirring for 3 h the reaction was quenched with ice and dissolved in DCM. The mixture was washed with brine and subjected to column chromatography (cyclohexane:ethyl acetate = 15:1 to 5:1) to obtain the desired product (71.2 mg, 0.072 mmol, 72 %). ^{1}H NMR (300 MHz, CD_2Cl_2) δ 7.07–6.76 (m, 48H), 2.20 (s, 3H), 1.77 (s, 6H). ^{13}C NMR (76 MHz, $CDCl_3$) δ 143.87, 143.82, 143.76, 143.72, 141.85, 141.16, 140.86, 140.73, 140.30, 138.19, 137.91, 137.08, 136.25, 135.59, 133.76, 131.58, 131.41, 131.37, 131.13, 129.43, 129.08, 128.93, 128.28, 127.69, 127.66, 127.61, 126.63, 126.52, 126.43, 125.88, 125.83, 125.35, 80.79, 24.24, 21.51, 20.66. MS (MALDI) calcd. $C_{93}H_{66}O^+$ [M^+] *m/z*: 986.4488; found: 986.4442.

2.7. 10-(di(pyren-1-yl)methylene)-9-(pyren-1-yl)-9,10-dihydroanthracen-9-ol (7)

1-Bromopyrene (168 mg, 0.60 mmol) was added to a dry reaction vessel with a magnetic stirring bar. After evacuating the flask three times, 3 mL of dry THF were added and the mixture was cooled down to −78 °C. 2.5 M n-BuLi (0.2 mL) was added dropwise, and the reaction mixture immediately turned to a yellow color. The mixture was stirred at the same temperature for 30 min. Compound **4** (93 mg, 0.15 mmol) in 5 mL of dry THF was added dropwise and the reaction was slowly let to warm up to room temperature. After further stirring for 3 h, the reaction was quenched with ice and dissolved in DCM. The mixture was washed with brine and subjected to column chromatography (cyclohexane: ethyl acetate 15:1 to 5:1) to obtain the desired product (103 mg, 0.13 mmol, 83 %). ^{1}H NMR (300 MHz, $CDCl_3$) δ 9.24 (dd, J = 13.6, 9.3 Hz, 2H), 9.08 (t, J = 9.3 Hz, 1H), 8.66 (d, J = 8.1 Hz, 1H), 8.48 (d, J = 8.1 Hz, 1H), 8.35–7.84 (m, 21H), 7.50 (d, J = 9.2 Hz, 2H), 7.38 (d, J = 7.4 Hz, 1H), 7.06 (d, J = 9.6 Hz, 1H), 6.79 (d, J = 7.5 Hz, 1H), 6.68 (t, J = 7.2 Hz, 1H), 6.60–6.41 (m, 4H. ^{13}C NMR (76 MHz, $CDCl_3$) δ 139.40, 136.59, 135.95, 131.63, 131.33, 131.11, 130.18, 129.37, 128.70, 128.55, 127.71, 127.61, 127.43, 127.28, 127.03, 126.49, 126.30, 126.21, 126.12, 125.85, 125.78, 125.44, 125.25, 125.06, 124.75, 124.36, 26.95. MS (MALDI) calcd. $C_{63}H_{36}O^+$ [M^+] *m/z*: 808.2766; found: 808.2778.

2.8. (10-Mesitylanthracen-9-yl)bis(4-(1,2,2-triphenylvinyl)phenyl) methanide (8)

Compound **6** (22.2 mg, 0.022 mmol) and $SnCl_2$•$2H_2O$ (8.0 mg, 0.035 mmol) were brought into a reaction vessel with a magnetic stirring bar. The vessel was evacuated and subsequently flooded with nitrogen three times. After this, degassed DCM (3 mL) was added and the mixture was stirred for 4 h at room temperature. This was followed by washing the reaction mixture with brine and subsequent column chromatography (cyclohexane: ethyl acetate 15:1 to 8:1) the product was obtained as a dark yellow solid (3.9 mg, 0.004 mmol, 18 %). MS (MALDI) calcd. $C_{76}H_{57}^{\bullet+}$ [M^+] *m/z*: 969.4460; found: 969.4437.

2.9. Di(pyren-1-yl)(10-(pyren-1-yl)anthracen-9-yl)methanide (9)

Compound **7** (21.5 mg, 0,026 mmol) and $SnCl_2$•$2H_2O$ (10.4 mg, 0.046 mmol) were brought into a reaction vessel with a magnetic stirring bar. The vessel was evacuated and subsequently flooded with nitrogen a total of three times. After this, degassed DCM (3 mL) was added and the mixture was stirred for 4 h at room temperature. This was followed by washing with brine and subsequent column chromatography (cyclohexane: ethyl acetate 15:1 to 8:1) to obtain the desired product (8.7 mg, 0.011 mmol, 42 %) as a dark red solid. MS (MALDI) calcd. $C_{63}H_{35}^{\bullet+}$ [M^+] m/z: 791.2739; found: 791.2781.

2.10. 2,2'-(Chloromethylene)bis(1,3,5-trichlorobenzene) (10)

1,3,5-trichlorobenzene (5.008 g, 27.60 mmol) and anhydrous aluminium chloride (3.672 g, 27.54 mmol) were put into a dry, sealed reaction vessel. After evacuation and flooding with nitrogen, dry chloroform (2.20 mL, 27.46 mmol) was added. The reaction mixture was stirred at 80 °C for 3 h. After the solution was let to cool to room temperature, it was poured over 1 M hydrochloric acid and extracted with

DCM. The solvent was reduced under vacuum and the raw product was washed with cold DCM to yield the desired product compound **10** (3.390 g, 8.28 mmol, 60 %) as a colorless solid. Impure fractions were purified via column chromatography with n-hexane. ^{1}H NMR (300 MHz, $CDCl_3$) δ 7.40–7.33 (m, 4H), 7.05–6.99 (m, 1H); ^{13}C NMR (76 MHz, $CDCl_3$) δ 136.86, 134.94, 132.13, 129.93, 128.56, 55.45. MS (DIP-EI) calcd. $C_{13}H_5Cl_6^+$ [M^+] *m/z*: 372.8488; found: 372.8488.

2.11. 2,2'-((2,4,6-)methylene)bis(1,3,5-trichlorobenzene) (11)

Compound **10** (1519 mg, 3.71 mmol) and 1,3,5-tribromobenzene (2309 mg, 7.33 mmol) and anhydrous aluminium chloride (544 mg, 4.08 mmol) are added to a dry reaction vessel. After evacuation and flooding with nitrogen, the mixture is put in an oil bath at 120 °C for 2 h. The reaction was let to cool to room temperature and after the addition of 1 M HCl, the product was extracted with DCM. The raw product was purified via column chromatography with n-hexane as eluent as a colorless solid. (1401 mg, 2.04 mmol, 64 %). ^{1}H NMR (300 MHz, $CDCl_3$) δ 7.74 (d, $J = 1.8$ Hz, 1H), 7.65 (d, $J = 1.8$ Hz, 1H), 7.41–7.32 (m, 2H), 7.23 (dd, $J = 4.3$, 2.1 Hz, 2H), 6.60 (s, 1H). ^{13}C NMR (76 MHz, $CDCl_3$) δ 138.57, 138.00, 137.48, 137.44, 136.91, 136.66, 136.49, 135.24, 134.02, 133.94, 133.88, 130.08, 129.80, 128.55, 128.40, 127.94, 126.76, 121.58, 54.16. MS (DIP-EI) calcd. $C_{19}H_7Cl_6Br_3^+$ [M^+] *m/z*: 687.6155; found: 687.6151.

2.12. : 4-((2,4,6-trichlorophenyl)methyl)-4'-(1,2,2-triphenylvinyl)-1,1'-biphenyl (12)

Compound **11** (627.6 mg, 0.913 mmol) and [4-(triphenylvinyl) phenyl] boronic acid pinacol ester (421.5 mg, 0.919 mmol) were brought into a reaction vessel which was evacuated and flooded with nitrogen twice. After this, Pd $(PPh_3)_4$ (123 mg, 0.106 mmol) was added and the vessel was again evacuated and flooded with nitrogen. The solvent (toluene (18 mL), ethanol (6 mL), 2 M K_3PO_4 solution (10.8 mL)) added and the reaction mixture was heated to 50 °C for 72 h. The reaction was quenched with the addition of 1 M hydrochloric acid and was extracted with DCM. The raw product was purified via column chromatography (n-hexane:chloroform 20:1 to 3:1) to yield compound **12** in two fractions of 586 mg total. One of these fractions contained no bromines (29 mg, 0.037 mmol, 4 %) and was used for further synthesis and characterization. The second fraction still had one bromine attached (430 mg, 0.502 mmol, 55 %). A mixture of the two fractions, which was not separable was also obtained (127 mg, 0.155 mmol, 17 %). ^{1}H NMR (300 MHz, CD_2Cl_2) δ 7.81 (d, $J = 1.2$ Hz, 1H), 7.45–7.29 (m, 7H), 7.10 (dd, $J = 9.9$, 6.0 Hz, 18H), 6.93 (d, $J = 8.1$ Hz, 1H), 6.61 (s, 1H). ^{13}C NMR (76 MHz, CD_2Cl_2) δ 171.19, 144.12, 144.09, 144.07, 144.04, 141.96, 141.90, 140.78, 137.87, 137.03, 136.67, 134.59, 134.04, 132.29, 132.23, 131.66, 131.60, 131.06, 129.81, 128.20, 128.12, 128.06, 126.99, 126.93, 126.89, 126.46, 126.18, 126.04, 60.64, 52.36, 32.01, 30.12, 23.08, 21.20, 14.44, 14.32. MS (MALDI) calcd. $C_{45}H_{28}Cl_6^+$ [M^+] *m/z*: 778.0322; found: 778.0338.

2.13. 6-(4-(Bis(2,4,6-trichlorophenyl)methyl)phenyl)-1,5a^1-dihydropyrene (13)

Compound **11** (356.1 mg, 0.512 mmol) and pyren-1-ylboronic acid (134.9 mg, 0.548 mmol) were brought into a reaction vessel which was evacuated and flooded with nitrogen twice. After this, $Pd(PPh_3)_4$ (81.7 mg, 0.0707 mmol) was added and the vessel was again evacuated and flooded with nitrogen. The solvent (toluene (13.5 mL), ethanol (2.25 mL), 2 M Na_2CO_3 solution (4.5 mL)) were added and the reaction mixture was heated to 50 °C for 48 h. The reaction was quenched with the addition of 1 M hydrochloric acid and was extracted with DCM. The raw product was purified via column chromatography to yield compound **13** (207 mg, 0.317 mmol, 62 %) as a colorless solid. ^{1}H NMR (300 MHz, CD_2Cl_2) δ 8.12 (dd, $J = 15.1$, 8.3 Hz, 6H), 8.02 (s, 3H), 7.98–7.87 (m, 4H), 7.53 (d, $J = 8.1$ Hz, 1H), 7.40–7.28 (m, 5H), 6.59 (s, 1H). ^{13}C NMR (76 MHz, CD_2Cl_2) δ 140.53, 140.46, 138.12, 138.05, 137.78, 137.70, 137.60, 137.51, 136.35, 135.50, 134.05, 133.94, 133.83, 133.67, 131.98, 131.89, 131.38, 131.25, 131.10, 131.02, 130.12, 129.94, 129.68, 129.62, 128.83, 128.03, 127.88, 127.79, 127.53, 127.18, 126.48, 125.54, 125.27, 125.20, 125.11, 125.06, 51.84, 50.80, 37.49, 33.17, 32.36, 30.45, 30.12, 29.79, 27.49, 23.12, 14.31. MS (MALDI) calcd. $C_{35}H_{20}Cl_6^+$ [M^+] *m/z*: 649.9696; found: 649.9631.

2.14. (4'-(Bis(2,4,6-trichlorophenyl)methyl)-3'-bromo-2,4,6-trimethyl-1,1'-biphenyl) (14)

Compound **11** (54.5 mg, 0.079 mmol) and 2,4,6 trimethylphenylboronic acid (16.8 mg, 0.102 mmol) were brought into a reaction vessel which was evacuated and flooded with nitrogen twice. After this $Pd(PPh_3)_4$ (10.4 mg, 0.009 mmol) was added and the vessel was again evacuated and flooded with nitrogen. The solvent mixture, consisting of toluene (3 mL), ethanol (0.5 mL) and 2 M Na_2CO_3 solution (1 mL), was added and the reaction mixture was heated to 50 °C for 48 h. The reaction was quenched with the addition of 1 M hydrochloric acid and was extracted with DCM. The raw product was purified via column chromatography to yield compound **14** as a colorless solid. A mixture of the product with one bromine and no bromines was obtained. ^{1}H NMR (300 MHz, $CDCl_3$) δ 7.35 (d, $J = 6.4$ Hz, 5H), 6.94 (d, $J = 5.5$ Hz, 4H), 6.64 (s, 1H), 2.32 (s, 3H), 2.00 (s, 6H). MS (APCI) calcd. $C_{28}H_{19}BrCl_6^+$ [M^+H^+] *m/z*: 644.89 found: 644.7. MS (APCI) calcd. $C_{28}H_{20}Cl_6^+$ [M^+H^+] *m/z*: 566.98 found: 566.8.

2.15. Bis(2,4,6-trichlorophenyl)(4'-(1,2,2-triphenylvinyl)-[1,1'-biphenyl]-4-yl)methanide (15)

Compound **12** (23.4 mg, 0.0299 mmol) is dissolved in dry THF and the reaction vessel is purged with nitrogen. Then, 1 M tetrabutylammonium hydroxide (TBAH) in methanol (0.06 mL, 2 equiv.) was added and the mixture was stirred in the dark overnight at room temperature. This was followed by the addition of *p*-chloranil (39.5 mg, 0.161 mmol) and the mixture was again stirred for 3 h in the dark. The reaction was stopped and the THF was removed under vacuum. The product was redissolved in DCM and washed with brine. This was followed by column chromatography (n-hexane:chloroform 20:1 to 3:1) to obtain compound **15** (14.2 mg, 0.0182 mmol, 61 %). MS (MALDI) calcd. $C_{45}H_{27}Cl_6^{\bullet+}$ [M^+] *m/z*: 777.0244; found: 777.0236.

2.16. (4-(3a^1,6-Dihydropyren-1-yl)phenyl)bis(2,4,6-trichlorophenyl) methanide (16)

Compound **13** (21.6 mg, 0.0331 mmol) is dissolved in dry THF and the reaction vessel is purged with nitrogen. The 1 M tetrabutylammonium hydroxide (TBAH) in methanol (0.07 mL, 2 equiv.) was added and the mixture was stirred in the dark overnight at room temperature. This was followed by the addition of *p*-chloranil (45.6 mg, 0.186 mmol) and the mixture was again stirred for 3 h in the dark. The reaction was stopped and the THF was removed under vacuum. The product was redissolved in DCM and washed with brine. This was followed by column chromatography (n-hexane:chloroform 20:1 to 3:1) to obtain compound **16** as a dark yellow solid (15.1 mg, 0.0232 mmol, 70 %). MS (MALDI) calcd. $C_{35}H_{19}Cl_6^{\bullet+}$ [M^+] *m/z*: 648.9618; found: 648.9619.

3. Results and discussion

The synthesis of the light-emitting radicals was achieved via two different synthetic pathways: The first one with an anthracene at the core and the second one with a trityl core structure. In the case of the anthracene scheme (Fig. 3), three precursors (compounds **5–7)** and two final radicals were obtained (compounds **8** and **9**).

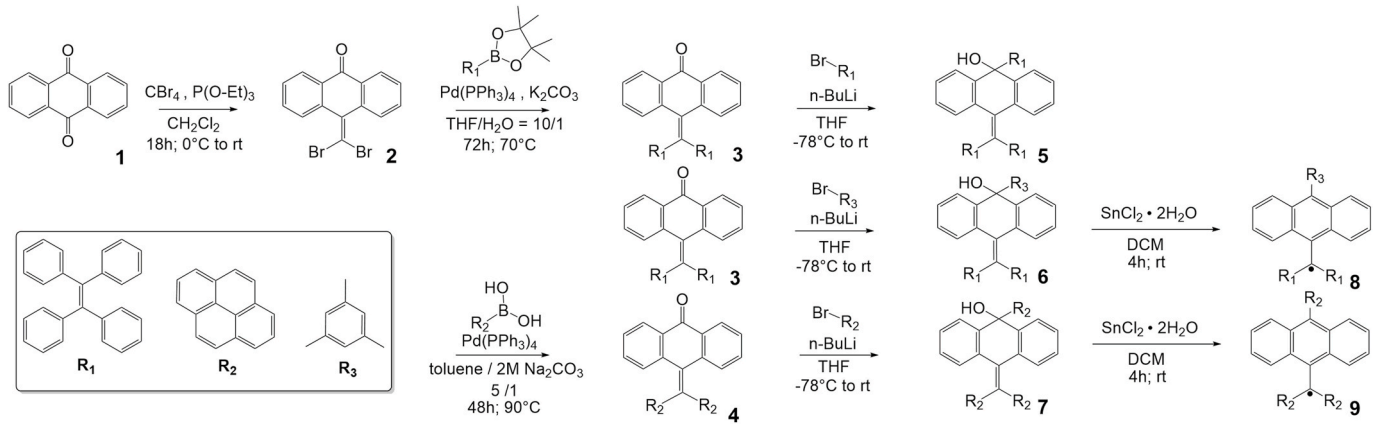

Fig. 3. Overview of the reactions of the anthracene synthesis scheme.

3.1. Preparation of the anthracene-core radicals

The initial step of the anthracene scheme was straightforward and worked well. After a Corey-Fuchs reaction on only one of the anthraquinone carbonyl groups, two different Pd-catalyzed coupling methods were used on compound **2**, namely Suzuki-, and Buchwald-Hartwig coupling. Out of these, only the Suzuki coupling was able to deliver decent yields, especially the synthesis with the boronic ester worked excellent with the boronic acid reaction showing lower yields in comparison. The products obtained from the Buchwald-Hartwig coupling were in a large part only mono-substituted compounds and thus this route was ultimately abandoned.

The addition of the bromo derivatives of mesitylene, TPE and pyrene via n-BuLi on the other side of the anthracene core of the reagents worked well in all cases after some troubleshooting, since a stabilizer present in the THF hindered the formation of the intermediate ions.

The final radicalization step of this synthesis was the simplest to set up since no heating, inert and dry conditions or any other kind of fine-tuning was necessary. $SnCl_2$ was used as reducing agent and compounds **8** and **9** were obtained with a decent yield. Only for precursor compound **5**, it was not possible to obtain the final radical. This may be explained due to the high flexibility of the bond from the TPE to the anthracene core and following the low shielding ability of the TPE moiety for the radical. This is also evident in the lower yield of compound **8**.

3.2. Preparation of the trityl-core radicals

For the trityl pathway (Fig. 4), also three precursors (compounds **12–14**) and two final products were synthesized (compounds **15** and **16**). The first two steps were done according to the literature [29], yielding similar results and leading to compound **11**. The initial idea of getting bromines in meta-position with *2,4-dibromomestiylene* was not successful. This is most likely due to the electron-pushing of the bromines not allowing to attach any bond to the unoccupied phenyl carbon at the meta-position.

In this scheme also a Suzuki-coupling was carried out with either the boronic acid or the boronic pinacol ester of mesitylene, TPE and pyrene. The reactions had to be carried out under light exclusion, and again the ester yieled better results. This may be due to the lower stability of the boronic acid, making them easily oxidized and thus leading to unwanted side reactions. We observed this instability, as there was a large fraction of pyrene, which was separable only by column chromatography.

A major problem however occurred with the already attached bromines in ortho-position, as reported before [29], also we observed a loss of either one, or in most cases both of these bromines. This is probably

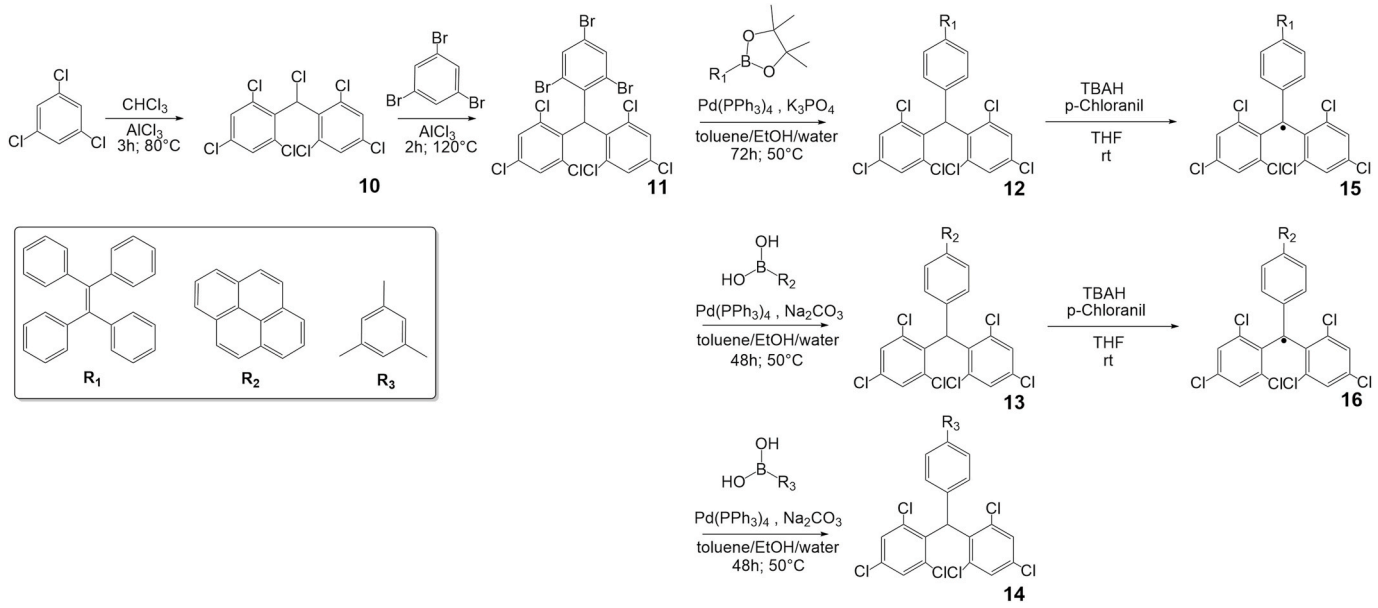

Fig. 4. Overview of the reactions of the trityl synthesis scheme.

due to the Pd-catalyst carrying out a reductive elimination and thus removing bromine. Due to the steric hindrance of the chlorine atoms on the other phenyl rings, the catalytic cycle cannot run through fully and leaves the ortho-position unoccupied reducing the overall stability, leaving only hydrogen attached instead of bromine [30]. An attempt to get rid of the remaining bromine in the single-bromo-species by letting it react with the catalyst did not yield any promising results.

Three radical precursors were made, of which only the fractions without bromines of two of these molecules were used for the final step, thus allowing for an easier comparison and subsequent characterization. The radicalization is a two-step reaction and uses TBAH to extract the α-hydrogen from the central carbon to yield the anion. In addition, p-chloranil is needed as electron acceptor to yield the radical. This reaction required more sophisticated conditions, as it had to be done, not only under light exclusion, but also in inert and dry conditions. However, we were able to obtain the two attempted products, compounds **15** and **16** in a decent yield.

By making a comparison of both synthetic schemes we carried out, it is evident that the anthracene scheme is the favorable one. Firstly, we reduce the need for halogens in the final structure. Secondly, the overall reactions and especially the work-up of the products worked well and are much easier to carry out. This is especially evident in the final step, where the loss of the –OH group allows for a significant change in polarity in the anthracene scheme. In the case of the trityl synthesis scheme, the educts and products are structurally often similar, making it difficult to separate them with commonly used techniques. Thirdly, the final products of the anthracene scheme appear to be more stable, even after several weeks of storage in the freezer at −18 °C, they did not show any significant deterioration. The trityl-core radicals on the other hand appeared to be instable.

3.3. EPR spectroscopy

The obtained EPR spectra for all of the radicals (compounds **8**, **9**, **15** and **16**) show a clear signal (Fig. 5 and Fig. S37, 38), thus confirming the presence of an unpaired electron in their respective structures. The g-values were calculated versus 1,1-diphenyl-2-picrylhydrazyl (DPPH) as a reference and are summarized in Table 1. They are all shifted to higher values when compared the free electron at 2.0023 and are within the expected range of organic radicals (1.99–2.01) [31].

The absorption is influenced by neighboring magnetic nuclei, resulting in distinct hyperfine couplings for the compounds **8**, **15** and **16**. It was, however, not possible to determine the exact structural reason for the hyperfine couplings from the obtained data. In the case of the anthracene-type radicals, the most stable compound **9** did not show any hyperfine coupling, but only displayed a broad single signal. Additionally, also for the trityl-type radicals, only the more stable structure of compound **15** (Fig. 5), displays a weak coupling. This could mean that the radical is either localized on the α-carbon atom in the center or delocalized over the entire molecular structure [32].

Table 1
The g-values of the synthesized radicals.

Compound	8	9	15	16
g-value	2.0069	2.0058	2.0092	2.0088

3.4. Photophysical characterization

In order to determine the photophysical properties of the synthesized radicals, UV–Vis absorption and fluorescence emission spectra were recorded and quantum yields were determined. For all measurements in solution, a stock solution with a concentration of 0.5 μM of the radicals was prepared in HPLC gradient THF of which 30 μL were put into a quartz cuvette. The solid-state samples for UV–Vis spectroscopy and fluorescence measurements were prepared via spin-coating 50 μL of a 10 mg/mL solution of the radicals onto a 15 × 15 mm glass substrate. For the quantum yield measurements with an integrating sphere, 20 μL of the same solution were spin-coated onto another 5 × 5 mm glass substrate. This was necessary due to the size limitations of the instrument.

We focused on the comparison of the UV–Vis absorption spectra of the radical species in solution and in solid-state (Fig. 6). The UV–Vis spectra were measured in a range from 200 nm to 1100 nm. Above 800 nm, no absorption peaks were observed for any of the prepared samples, hence the plotted range was cut off beyond this wavelength.

In general, the samples in solution absorb at a higher wavelength, ranging up to 600 nm in the case of the anthracene core structure radicals and even up to almost 700 nm for the trityl core structure radicals. The obtained data can be found in Table 2.

For the trityl radicals, the absorption at around 360 nm originates from the π–π* transitions of the trityl core [33], whereas the absorption at higher wavelengths of 500 nm–700 nm can be attributed to the charge-transfer (CT) between the electron donor substitutes and the trityl moiety [34]. In the case of the TPE substituted radical, the absorption at the highest wavelength has its maximum at 650 nm and the pyrene substituted radical has its highest peak at 489 nm in solution with no significant absorption occurring above 400 nm in solid-state for neither of the samples.

The anthracene-type radicals also exhibit a strong absorption ranging from 330 nm to 370 nm. This is associated with the presence of the anthracene chromophore in the center of the molecule [35]. In this case, the signature absorption bands are redshifted when compared to the TTM radicals and blue shifted in comparison to the synthesized trityl counterparts of compounds **15** and **16** [36].

When looking at the TAntM radical, which has its maximum at 600 nm, a slight red-shift can be observed for compound **8** in solution with its maximum being located at 610 nm, whereas compound **9** shows a blue-

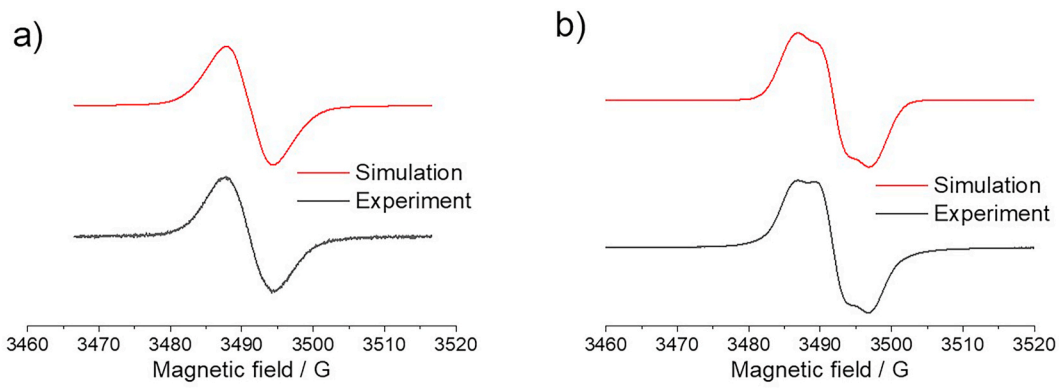

Fig. 5. EPR spectra of a) compound 9 and b) compound 15. The experimental spectra are shown in black and the simulated spectra are shown in red.

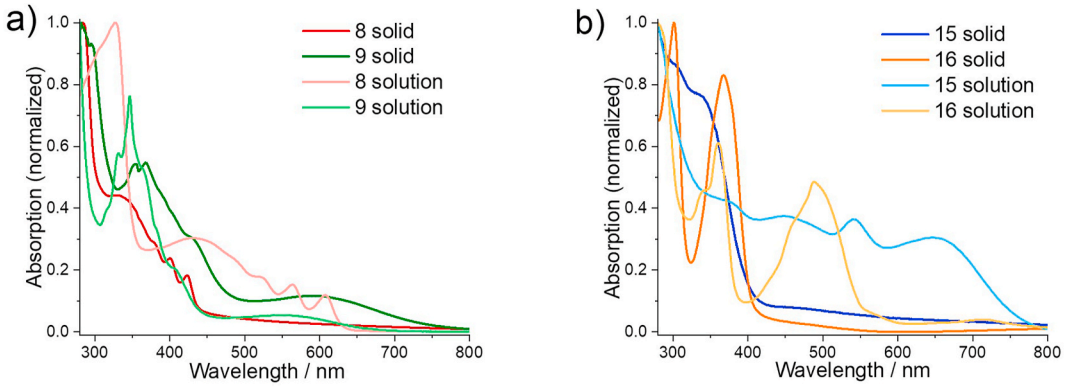

Fig. 6. UV–Vis spectra of the radicals: a) anthracene based compounds 8 and 9 and b) trityl based compounds 15 and 16 measured in solid state and solution.

Table 2
Obtained photoluminescence data of the synthesized radicals and their respective precursors. UV–Vis Absorption (λ_{Abs}), fluorescence emission (λ_{Em}), quantum yields (φ) in solution and in solid state and the molar absorption coefficient (ε).

Precursors	λ_{Abs} solution(nm)	λ_{Abs} solid(nm)	λ_{Em} solution(nm)	λ_{Em} solid(nm)	φ solution (%)	φ solid (%)	ε ($M^{-1}\cdot cm^{-1}$)
5	316	335	493	484	<0.1	22.8	33000
6	323	/	493	/	<0.1	21.8	25600
7	347	370	407/431	502	0.6	2.0	71200
12	323	349	388	477	<0.1	21.5	9830
13	344	367	383/399	467	19.1	47.7	42300
Radicals							
8	328/610	333/423	434	529	0.1	13.4	17000
9	347/554	368/592	442	471	3.0	10.1	33000
15	650	342	388/474	465	<0.1	11.1	11800
16	362/489	368	383/399	419/459	14.0	16.5	51000

shift to 554 nm [37].

Only compound **9** has a similar absorption spectrum in solution and in the solid-state with a slight blue-shift occurring from the solution to the solid-state and the absorption maxima being at 590 nm. For all of the other radicals, the absorption seems to fade away after 400 nm in solid-state with only a tail remaining, extending up to 600 nm with the maxima for the compounds **8** and **9** at 423 nm and 592 nm, respectively, hinting towards a loss of interaction in the solid state between the anthracene and trityl core with the respective substitutes.

The fluorescence emission spectra (Fig. 7) were measured with an excitation wavelength of 350 nm and the spectra were recorded from 365 nm and after 650 nm no significant peaks were observed. Also, in this case we compared the solution and solid-state samples.

As reported, there is a hypsochromic shift when fewer bromine atoms are present in the trityl structure [29]. Both the compounds **15** and **16** without any bromines display a yellow color, whereas the brominated trityl derivative radical has a distinct red color. This shift, however, is a tradeoff with the decreasing stability of the radical, since fewer halogens mean a lower steric hindrance [29]. Compound **15** has its fluorescence emission maximum at 474 nm in solution and 465 nm in solid-state. Compound **16** shows a maximum at 383 nm in solution with a shoulder at 399 nm and at 419 nm in solid-state with a shoulder at 459 nm.

Taking a closer look at the two anthracene radicals and comparing them to the TAntM radical by Kubo et al., which has an intense absorption at 600 nm, a hypsochromic shift is evident [27,37]. Compound **8** has its emission maximum at 434 nm (solution) and 529 nm (solid-state) and compound **9** at 442 nm (solution) and 471 nm (solid-state). All emission peaks extend until 600 nm and beyond.

All of the measured radicals displayed fluorescence emission in solution and in solid-state. Compounds **8** and **16** showed a red shift in the

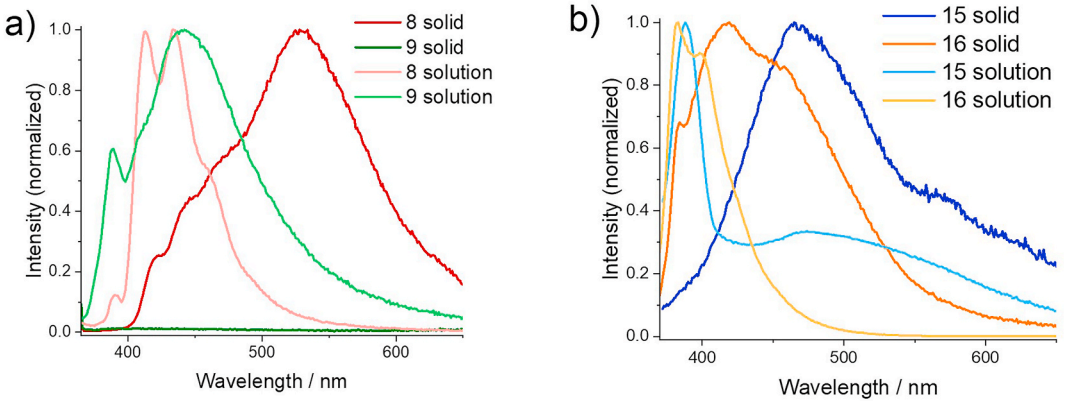

Fig. 7. Fluorescence emission spectra of the radicals: a) anthracene based compounds 8 and 9 and b) trityl based compounds 15 and 16 measured in solid state and solution with an excitation wavelength of 350 nm.

solid-state and compound **15** was slightly shifted towards the blue region. Comparing these results to the TTM radical, with its emission maxima being at 565 nm, a significant blue-shift is observable for both the solution and the solid-state samples [38].

This is even more pronounced, when looking at TTM radicals with an electron-donor group attached, such as carbazole, which has its photoluminescence maxima at 678 nm [39].

Depending on the donor strength, the substitute changes the fluorescence quantum yield of the radicals. To determine their influence on the ratio of the radiative decay rate to the non-radiative decay of the synthesized radical fluorophores, the quantum yield was measured with an integrating sphere.

For the radicals, there is no clear trend observable between the solution and the solid-state. Compound **8** has a quantum yield of 13 % in solid-state and compound **15** shows a little lower value of 11 %. One observation, however, can be made when looking at the compounds **8** and **15**. The comparatively low PLQYs of the radicals are consistent with the intrinsic limitations of radical emitters, including low oscillator strengths and competing non-radiative decay channels. A more detailed comparison of radiative and non-radiative decay rates, via lifetime measurements, is valuable but lies beyond the scope of the present work. Both radicals show a ten-fold increase of quantum yield in the solid-state, confirming the AIE nature of the radicals. The enhancement of PLQY in the solid state compared to solution can be explained by the suppression of intramolecular motions and the absence of solvent quenching, which together reduce non-radiative decay channels. Furthermore, the quantum yields could be improved in the future by using a suitable matrix.

3.5. Theoretical calculations

We carried out preliminary geometry optimizations adopting the GFN2-xTB model available in the xTB software [40,41]. Subsequent calculations were all performed with the Gaussian16 software [42], which we used to carry out DFT/B3LYP-D3BJ/def2-SVP ground state geometry optimizations in vacuo, characterizing stationary points through calculations of vibrational frequencies, which were all positive. We finally proceeded to obtain excited state properties (for the first 12 excited states) at TDDFT/M06-2X/def2-TZVPP level including solvation effects for THF through the polarizable continuum model (PCM) in its integral equation formalism [43]. We also computed electronic properties at the excited state minimum geometry, corresponding to experimental fluorescence measurements. S1 equilibrium geometries and electronic properties were obtained at the TDDFT/M06-2X/def2-TZVPP for compounds **15** and **16**, and TDDFT/M06-2X/def2-SVP for compounds **8** and **9** due to their larger size.

For radicals described in this work, namely compounds **8**, **9**, **15**, and **16**, we carried out an extensive computational characterization of the electronic properties of such dyes. The main spectroscopic data obtained from our computational analyses are summarized in Table 3, while the complete characterization of light absorption and emission properties (with assignments of transitions) is reported in the Supporting Information. In the spectral region spanned by the first 12 excited states we computed, several moderately intense transitions appear for all substrates. Fig. 8 displays the relative energy levels and the spatial distribution of the respective orbitals. Indicating the differing electronic coupling and transition characteristics.

Table 3
Absorption and emission wavelengths for the first bright transitions, and oscillator strengths for radicals computed at TDDFT/M06-2X/def2-TZVPP, including THF solvation through IEF-PCM.

Radicals	λ_{Abs} (nm)	λ_{Em} (nm)	f_{Abs}
8	441	/	1.14
9	539	/	0.41
15	467	586	0.09
16	534	/	0.02

For compound **8**, the two lowest excited states are dark, and the first bright one is computed at 441 nm (f ~ 1.14), in fair agreement with the experimental signal of the solid state spectrum at 423 nm reported in (Fig. 6). This state involves a combination of SOMO → LUMO (α spin) and HOMO → SUMO (β spin) transitions, with orbitals localized on the two TPE moieties connected to the radical center, explaining the large oscillator strength computed. All the other states we computed for this dye show almost negligible oscillator strengths (see Supporting Information), hinting at transitions involving orbitals localized on different portions of the dye.

For compound **9**, the first three states are dark, and the first bright one is located at 539 nm (f ~ 0.41). The orbitals involved in the transitions are localized mostly on the two pyrene moieties directly connected to the radical center, with small contributions of orbitals on the anthracene spacer (Fig. 8). Transitions localized mostly on the anthracene spacer contribute, instead, to the second bright state, located nearby at 524 nm (f ~ 0.39). These two states should be responsible for the broad absorption band observed experimentally above 500 nm in solution (see Fig. 6).

The lowest energy transition for compound **15** is predicted at 467 nm, mostly a HOMO-1 → LUMO (β spin) transition. The HOMO-1 is mostly localized on the trityl, with a little contribution of atomic orbitals belonging to the TPE moiety. The LUMO is mostly localized on the TPE, confirming the assignment to a CT transition (Fig. 8). The small overlap between orbitals involved in the transition results in a moderate oscillator strength (f ~ 0.1, proportional to the intensity of the spectrum), also confirming the CT nature of this state, which should be responsible for the tail observed above 450 nm in the absorption spectra (Fig. 6). In the Supporting Information, we show that transitions from 377 to 365 nm are instead associated to large oscillator strengths (f up to 0.45), and are the bright transitions experimentally measured in the same spectral region at 342 nm. Orbitals involved in these transitions are localized on the trityl moiety.

For compound **16**, the first excited state (at 534 nm) shows a low absorption capability (f ~ 0.02), with orbitals localized on the phenyl spacer and pyrene moieties. The next two bright states, instead, appear at 454 nm and 395 nm (f ~ 0.24 and f ~ 0.43, respectively), and they are both described by a combination of transitions localized on either the pyrene or the trityl moieties (see Supporting Information). In this case, the computed transition wavelengths seem to underestimate the experimental spectrum, which shows a maximum at 489 nm in solution.

4. Conclusion

In a nutshell, the synthesis of new open-shell molecules, displaying fluorescence activity in the solid state, was successfully carried out via two different pathways. Of these two synthetic routes, the anthracene-based moieties appear to be more promising regarding the future development of these types of materials and their potential usage in OLEDs due to an overall more efficient synthesis, which also allows for an easier implementation of different side groups. All final compounds demonstrated both photoluminescent and paramagnetic characteristics, with fluorescence emissions spanning from 383 to 529 nm and solid-state quantum yields of up to 16.5 %. Compared to conventional OLED emitter classes such as fluorescent, phosphorescent, and TADF systems, our radical-based emitters currently show lower PLQYs. Nevertheless, they offer the unique advantage of doublet-spin emission, which in principle allows for 100 % IQE without the need for heavy metals, highlighting their potential as a complementary class of emitting materials. These findings underscore the strong potential of this strategy for creating a new class of fluorophores tailored for high-performance OLED applications. In further studies, integration of these materials into the emissive layer of OLEDs along with comprehensive evaluation of their photophysical properties and operational lifetimes will be

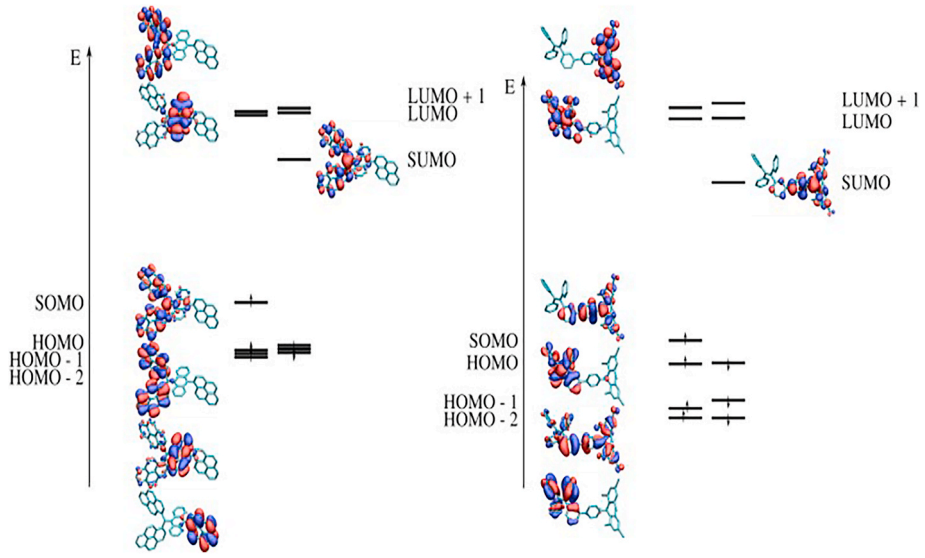

Fig. 8. Frontier molecular orbitals for compound 9 and compound 15.

essential to fully understand their properties and to assess their performance and applicability in real-world applications.

CRediT authorship contribution statement

Marco Zechner: Writing – review & editing, Writing – original draft, Validation, Investigation, Formal analysis. **Suman Mallick:** Writing – review & editing, Writing – original draft, Supervision, Project administration, Investigation, Funding acquisition, Conceptualization. **Max Schmallegger:** Writing – original draft, Formal analysis, Data curation. **Daniele Padula:** Writing – original draft, Formal analysis, Data curation. **Thomas Rath:** Writing – review & editing, Writing – original draft, Validation, Project administration, Investigation. **Gregor Trimmel:** Writing – review & editing, Writing – original draft, Validation, Supervision, Project administration, Investigation, Formal analysis.

Declaration of competing interest

The authors declare that they have no known competing financial interests or personal relationships that could have appeared to influence the work reported in this paper.

Acknowledgment

The authors sincerely thank the group of Assoc. Prof. Sergey Borisov for allowing us to use the fluorescence spectrometer and want to mention that the TU Graz Initial Funding Program (18th call) provided the necessary financial support to carry out the project.

Appendix A. Supplementary data

Supplementary data to this article can be found online at https://doi.org/10.1016/j.dyepig.2025.113329.

Data availability

Data will be made available on request.

References

[1] Chen ZX, Li Y, Huang F. Persistent and stable organic radicals: design, synthesis, and applications. Chem 2021;7:288–332. https://doi.org/10.1016/j.chempr.2020.09.024.
[2] Thilagam A. Effect of the Pauli exclusion principle on the singlet exciton yield in conjugated polymers. Appl Phys A Mater Sci Process 2016;122:1–7. https://doi.org/10.1007/s00339-016-9792-5.
[3] Law CK. Quantum entanglement as an interpretation of bosonic character in composite two-particle systems. Phys Rev A - At Mol Opt Phys 2005;71:1–4. https://doi.org/10.1103/PhysRevA.71.034306.
[4] Uoyama H, Goushi K, Shizu K, Nomura H, Adachi C. Highly efficient organic light-emitting diodes from delayed fluorescence. Nature 2012;492:234–8. https://doi.org/10.1038/nature11687.
[5] Luo J, Rong XF, Ye YY, Li WZ, Wang XQ, Wang W. Research progress on Triarylmethyl radical-based high-efficiency OLED. Molecules 2022;27:1632. https://doi.org/10.3390/molecules27051632.
[6] Kim JW, Yoo S Il, Kang JS, Yoon GJ, Lee SE, Kim YK, et al. Quenching in single emissive white phosphorescent organic light-emitting devices. Org Electron 2016;38:230–7. https://doi.org/10.1016/j.orgel.2016.08.020.
[7] Strassner T. Phosphorescent Platinum(II) complexes with CˆC* cyclometalated NHC ligands. Acc Chem Res 2016;49:2680–9. https://doi.org/10.1021/acs.accounts.6b00240.
[8] Di D, Romanov AS, Yang L, Richter JM, Rivett JPH, Jones S, et al. High-performance light-emitting diodes based on carbene-metal-amides, 163; 2017. p. 159–63.
[9] Wong MY, Zysman-Colman E. Purely organic thermally activated delayed fluorescence materials for organic light-emitting diodes. Adv Mater 2017;29:1605444. https://doi.org/10.1002/adma.201605444.
[10] Adachi C, Baldo MA, Thompson ME, Forrest SR. Nearly 100% internal phosphorescence efficiency in an organic light emitting device. J Appl Phys 2001;90:5048–51. https://doi.org/10.1063/1.1409582.
[11] Peng Q, Obolda A, Zhang M, Li F. Organic light-emitting diodes using a neutral π radical as emitter: the emission from a doublet. Angew Chem Int Ed 2015;54:7091–5. https://doi.org/10.1002/anie.201500242.
[12] Gamero V, Velasco D, Latorre S, López-Calahorra F, Brillas E, Juliá L. [4-(N-Carbazolyl)-2,6-dichlorophenyl]bis(2,4,6-trichlorophenyl)methyl radical an efficient red light-emitting paramagnetic molecule. Tetrahedron Lett 2006;47:2305–9. https://doi.org/10.1016/j.tetlet.2006.02.022.
[13] Müllegger S, Rashidi M, Fattinger M, Koch R. Surface-supported hydrocarbon π radicals show Kondo behavior. J Phys Chem C 2013;117:5718–21. https://doi.org/10.1021/jp310316b.
[14] Ratera I, Vidal-Gancedo J, Maspoch D, Bromley ST, Crivillers N, Mas-Torrent M. Perspectives for polychlorinated trityl radicals. J Mater Chem C 2021;9:10610–23. https://doi.org/10.1039/d1tc02196f.
[15] Gao S, Cui Z, Li F. Doublet-emissive materials for organic light-emitting diodes: exciton formation and emission processes. Chem Soc Rev 2023;52:2875–85. https://doi.org/10.1039/d2cs00772j.
[16] Ai X, Evans EW, Dong S, Gillett AJ, Guo H, Chen Y, et al. Efficient radical-based light-emitting diodes with doublet emission. Nature 2018;563:536–40. https://doi.org/10.1038/s41586-018-0695-9.
[17] Abroshan H, Coropceanu V, Brédas JL. Radiative and nonradiative recombinations in organic radical emitters: the effect of guest–host interactions. Adv Funct Mater 2020;30:1–10. https://doi.org/10.1002/adfm.202002916.
[18] Smeu M, Dilabio GA. Calculations of electron transport through simple π-and σ-type radicals. J Phys Chem C 2010;114:17874–9. https://doi.org/10.1021/jp105589y.
[19] Kusamoto T, Kume S, Nishihara H. Realization of SOMO-HOMO level conversion for a TEMPO-dithiolate ligand by coordination to platinum(II). J Am Chem Soc 2008;130:13844–5. https://doi.org/10.1021/ja805751h.
[20] Reineke S. Radically more stable. Nat Mater 2019;18:917–8.

[21] Guo H, Peng Q, Chen XK, Gu Q, Dong S, Evans EW, et al. High stability and luminescence efficiency in donor–acceptor neutral radicals not following the Aufbau principle. Nat Mater 2019;18:977–84. https://doi.org/10.1038/s41563-019-0433-1.
[22] Tanushi A, Kimura S, Kusamoto T, Tominaga M, Kitagawa Y, Nakano M, et al. Nir emission and acid-induced intramolecular electron transfer derived from a somo-homo converted non-Aufbau electronic structure. J Phys Chem C 2019;123:4417–23. https://doi.org/10.1021/acs.jpcc.8b08574.
[23] Abdurahman A, Hele TJH, Gu Q, Zhang J, Peng Q, Zhang M, et al. Understanding the luminescent nature of organic radicals for efficient doublet emitters and pure-red light-emitting diodes. Nat Mater 2020;19:1224–9. https://doi.org/10.1038/s41563-020-0705-9.
[24] Dong S, Xu W, Guo H, Yan W, Zhang M, Li F. Effects of substituents on luminescent efficiency of stable triaryl methyl radicals. Phys Chem Chem Phys 2018;20:18657–62. https://doi.org/10.1039/C8CP01492B.
[25] Ding J, Dong S, Zhang M, Li F. Efficient pure near-infrared organic light-emitting diodes based on tris(2,4,6-trichlorophenyl)methyl radical derivatives. J Mater Chem C 2022;10:14116–21. https://doi.org/10.1039/d2tc03299f.
[26] Murto P, Bronstein H. Electro-optical π-radicals: design advances, applications and future perspectives. J Mater Chem C 2022;10:7368–403. https://doi.org/10.1039/d1tc05268c.
[27] Nishiuchi T, Aibara S, Kubo T. Synthesis and properties of a highly congested Tri(9-anthryl)methyl radical. Angew Chem Int Ed 2018;57:16516–9. https://doi.org/10.1002/anie.201811314.
[28] Hudson JM, Hele TJH, Evans EW. Efficient light-emitting diodes from organic radicals with doublet emission. J Appl Phys 2021;129:180901. https://doi.org/10.1063/5.0047636.
[29] Chen L, Arnold M, Blinder R, Jelezko F, Kuehne AJC. Mixed-halide triphenyl methyl radicals for site-selective functionalization and polymerization. RSC Adv 2021;11:27653–8. https://doi.org/10.1039/d1ra04638a.
[30] Ahmadi Z, McIndoe JS. A mechanistic investigation of hydrodehalogenation using ESI-MS. Chem Commun 2013;49:11488–90. https://doi.org/10.1039/c3cc46271d.
[31] Woodward JR. Radical pairs in solution. Prog React Kinet Mech 2002;27:165–207. https://doi.org/10.3184/007967402103165388.
[32] Abdurahman A, Wang J, Zhao Y, Li P, Shen L, Peng Q. A highly stable organic luminescent diradical. Angew Chem Int Ed 2023;62:e202300772. https://doi.org/10.1002/anie.202300772.
[33] Lv K, Zhang M, Li F. Efficient radical-based near-infrared organic light-emitting diodes with an emission peak exceeding 800 nm. J Mater Chem C 2023;11:15892–7. https://doi.org/10.1039/d3tc03017b.
[34] Matsuda K, Xiaotian R, Nakamura K, Furukori M, Hosokai T, Anraku K, et al. Photostability of luminescent tris(2,4,6-trichlorophenyl)methyl radical enhanced by terminal modification of carbazole donor. Chem Commun 2022;58:13443–6. https://doi.org/10.1039/d2cc04481a.
[35] Ohta A, Hattori K, Kusumoto Y, Kawase T, Kobayashi T, Naito H, et al. Effects of alkoxy substitution on the optical properties of 9,10-anthraquinone and anthracene: 2,3,6,7-tetrapropoxy-substituted vs. 2,6-dipropoxy-substituted derivatives. Chem Lett 2012;41:674–6. https://doi.org/10.1246/cl.2012.674.
[36] Bromberg A, Meisel D. Photophysics of arylmethyl radicals at 77 K. Structure-photoreactivity correlation. J Phys Chem 1985;89:2507–13. https://doi.org/10.1021/j100258a017.
[37] Nishiuchi T, Ishii D, Aibara S, Sato H, Kubo T. Synthesis, properties and chemical modification of a persistent triisopropylsilylethynyl substituted tri(9-anthryl) methyl radical. Chem Commun 2022;58:3306–9. https://doi.org/10.1039/d2cc00548d.
[38] Dong S, Obolda A, Peng Q, Zhang Y, Marder S, Li F. Multicarbazolyl substituted TTM radicals: Red-shift of fluorescence emission with enhanced luminescence efficiency. Mater Chem Front 2017;1:2132–5. https://doi.org/10.1039/c7qm00273d.
[39] Cui Z, Abdurahman A, Ai X, Li F. Stable luminescent radicals and radical-based leds with doublet emission. CCS Chem 2020;2:1129–45. https://doi.org/10.31635/ccschem.020.202000210.
[40] Bannwarth C, Caldeweyher E, Ehlert S, Hansen A, Pracht P, Seibert J, et al. Extended tight-binding quantum chemistry methods. WIREs Comput Mol Sci 2021;11(2). https://doi.org/10.1002/wcms.1493.
[41] Bannwarth C, Ehlert S, Grimme S. GFN2-xTB-An accurate and broadly parametrized self-consistent tight-binding quantum chemical method with multipole electrostatics and density-dependent dispersion contributions. J Chem Theor Comput 2019;15(3):1652–71. https://doi.org/10.1021/acs.jctc.8b01176.
[42] Frisch MJ, Trucks GW, Schlegel HB, Scuseria GE, Robb MA, Cheeseman JR, et al. Gaussian 16. Wallingford, CT: Rev. C.01; 2016.
[43] Tomasi J, Mennucci B, Cammi R. Quantum mechanical continuum solvation models. Chem Rev 2005;105(8):2999–3093. https://doi.org/10.1021/cr9904009.